Limits of Linear Rate Coding of Dynamic Stimuli by Electroreceptor Afferents

Daniel Gussin,[1] Jan Benda,[2] and Leonard Maler[1]
[1]*Department of Cell and Molecular Medicine and Center for Neural Dynamics, University of Ottawa, Ottawa, Ontario, Canada; and* [2]*Institute for Theoretical Biology, Humboldt University, 10115 Berlin, Germany*

Gussin D, Benda J, Maler L. Limits of linear rate coding of dynamic stimuli by electroreceptor afferents. *J Neurophysiol* 97: 2917–2929, 2007. First published February 7, 2007; doi:10.1152/jn.01243.2006. We estimated the frequency-intensity (f-I) curves of P-unit electroreceptors using 4-Hz random amplitude modulations (RAMs) and using the covariance method (50-Hz RAMs). Both methods showed that P units are linear encoders of stimulus amplitude with additive noise; the gain of the f-I curve was, on average, 0.32 and 2.38 spikes·s^{-1}·μV^{-1} for the low- and high-frequency cutoffs, respectively. There were two sources of apparent noise in the encoding process: the first was the variability of baseline P-unit discharge and the second was the variation of receptor discharge due to variability of the stimulus slope independent of its intensity. The covariance method showed that a linear combination of eigenvectors representing the time-weighted stimulus intensity (E1) and its derivative (E2) could account for, on average, 92% of the total response variability; E1 by itself accounted for 76% of the variability. The low gain of the low-frequency f-I curve implies that detection of small (1 μV) signals would require integration over many receptors ($\sim$1,200) and time (200 ms); even then, signals that elicit behavioral responses could not be detected using rate coding with the estimated gain and noise levels. Weak signals at the limit of behavioral thresholds could be detected if the animal were able to extract E1 from the population of responding P units; we propose a tentative mechanism for this operation although there is no evidence as to whether it is actually implemented in the nervous system of these fish.

INTRODUCTION

Sensory signals are typically encoded by the patterns of spikes in a population of afferent fibers. Discovering the neural code for a sensory system requires both specifying a map between external signals and the resulting spike trains and demonstrating that downstream neural circuits can interpret or decode this mapping and therefore direct behavioral output (Perkel and Bullock 1968). The original suggestion by Lord Adrian (Adrian 1932) that the intensity of a stimulus is linearly encoded by the spike rate over a fairly long time window (rate coding) has dominated this field. For slowly changing signals, this code can be simply estimated by presenting constant stimuli of varying intensity and counting the spikes emitted over many seconds; this results in a simple spike frequency-intensity (f-I) curve that summarizes the putative code. The advantage of this encoding scheme is that decoding merely requires temporal summation of input over a time window set by the synaptic and postsynaptic membrane time constants.

However, this method of estimating stimulus encoding fails for dynamic signals and for neurons with time-dependent conductances (e.g., adapting currents). More sophisticated methods such as the use of the spike-triggered stimulus average (STA) to estimate the reverse correlation of signal and spike train response have also been employed to estimate the linear encoding of signals (Chacron et al. 2005a; Metzner et al. 1998; Wessel et al. 1996). However, there is typically no obvious decoding mechanism implied by these techniques.

In this paper, we analyze encoding in the electrosensory system of the weakly electric fish, *Apteronotus leptorhynchus*. These fish emit a continuous quasi-sinusoidal electric organ discharge (EOD); the species EOD frequency ranges from $\sim$600 to 1,000 Hz, and the amplitude varies with fish size, but the EOD of an individual fish has nearly constant amplitude and frequency (Moortgat et al. 1998). The electric field induced by the EOD is sensed by specialized cutaneous tuberous electroreceptors. The most abundant tuberous receptor is the P unit, and it discharges in a probabilistic manner to the upward phase of the baseline EOD oscillation. An important parameter characterizing P units is their *P* value, defined as the probability of P unit spiking per EOD cycle and estimated as the ratio of P-unit frequency to EOD frequency; *P* values typically range from $\sim$0.10 to 0.50 (*P* value = 0.10–0.60) (Bastian 1981a; Xu et al. 1994, 1996). The amplitude of the EOD can be modulated by both the presence of nearby objects (electrolocation) or the EOD of conspecifics (electrocommunication) (Bastian 1981a; Benda et al. 2005, 2006; Nelson 2005; Nelson et al. 1997); electrolocation induces low-frequency amplitude modulations (AMs) (typically <20 Hz) (Bastian 1981a; Nelson and MacIver 1999) while electrocommunication AMs can exceed 200 Hz (Bastian et al. 2001; Benda et al. 2006). These AMs of the baseline EOD are the dynamic sensory signals for the electrosensory system and cause the P-unit firing rate to vary proportionally. P units have been thoroughly studied and modeled by many investigators (Bastian 1981a; Benda and Herz 2003; Benda et al. 2005; Chacron et al. 2001, 2005a; Kreiman et al. 2000; Ludtke and Nelson 2006; Nelson et al. 1997; Ratnam and Nelson 2000; Wessel et al. 1996; Xu et al. 1996); P-units are rapidly adapting (Benda et al. 2005; Xu et al. 1996) and are typically studied using sinusoidal (SAMs) or random AMs (RAMs). The emerging consensus from these studies is that, over the natural range of AM intensities and frequencies, P units are linear encoders and can predict ≤80% of the AM. However, the reverse correlation and coherence

---

methods often used in these studies again do not point to obvious decoding strategies.

In this paper, we estimate the f-I curves of P units using techniques recently developed by Brenner et al. (2000). Classic f-I curves were constructed using low-frequency noise; these results lead to a simple model of linear encoding with additive noise. The noise appeared to be due to both the well documented variability of baseline P-unit discharge and the sensitivity of P units to the stimulus slope as well as its intensity. Although it is easy to envision the decoding of this response, our calculations show that the estimated noise levels would preclude the model from detecting weak electrosensory signals. High-frequency noise signals and the covariance method were also used to construct f-I curves. We found that P units responded to a linear combination of time-weighted averages of the signal intensity and its slope; these two variables accounted for almost all the P-unit response variability and the first feature (intensity) contributes most to the response. We conclude that the apparent noise in the response to the signal's intensity (classic f-I curve) is due, in part, to the variation of the signal slope. We suggest a mechanism such that, if the fish were able to decompose the P-unit response into its intensity and slope components, then it could then detect the very weak signals to which it is behaviorally responsive.

METHODS

This study used data from single-unit nerve recordings from adult gymnotiform weakly electric fish *Apteronotus leptorhynchus* (10–14 cm). Animals were housed in groups of 3–10 in 150-l tanks, and the temperature were maintained at ~28°C. A dose of 100 ppm MS-222 (tricaine methanosulfonate, Sigma, St Louis, MO) anesthetized the fish before surgical and experimental procedures; the fish were then immobilized with an intramuscular injection of pancuronium bromide (Sigma) and placed in a water tank (46.5 × 41 × 18.5 cm) kept at 28°C and respirated with a constant flow of oxygenated water. The water resistivity of the water was typically set at ~4.5 kΩ cm to match that of the fish's home tank. All experimental protocols were approved by the University of Ottawa Animal Care Committee.

Experimental procedures were as previously reported (Benda et al. 2005). The posterior branch of the anterior lateral line ganglion (innervating trunk electroreceptors) was exposed and glass micropipettes (90–115 MΩ) advanced through the nerve with a piezoelectric microdrive (Inchworm IW-711, Burleigh, Fishers, NY). Action potentials were recorded (Axoprobe 1A; Axon Instruments, Union City, CA), band-pass filtered (0.3–7 kHz: PC1; TDT, Alachua, FL), and notch filtered at the fish's EOD frequency (Ultra-Q Pro; Behringer, Willich, Germany).

Two vertical carbon rods (11 cm long, 8 mm diam) recorded the unperturbed EOD between the head and tail of the fish. Stimuli (see following text) were attenuated (PA4; TDT, Alachua, FL), isolated (Model 2002; A-M Systems, Carlsborg, WA) and, for global stimulation, delivered by two stimulation electrodes (30-cm-long, 8-mm-diam carbon rods) parallel to its longitudinal axis and placed 15 cm on either side of the fish. Local stimulation by 20-Hz sine waves was delivered by two stimulation electrodes (0.005-in diam, 99.95% tungsten wire, California Fine Wire, Grover Beach, CA) 4 mm apart, parallel to the fish's longitudinal axis, and placed within 1 cm of the fish's surface; a 20% contrast was used. These local stimulation electrodes had their position adjusted to produce a maximal response from the receptor and we assumed that this identified its location. During both global and local stimulation, two chloridized silver wires insulated up to their tips with nail polish and 4 mm apart recorded the field gradient adjacent to the animals skin. These silver wires were oriented perpendicular to the global stimulation electrodes at the site of maximal response to local stimulation and thus measured the stimulus delivered to the recorded P-unit. The EOD and field gradient were amplified and low-pass filtered (5 kHz; 2015F, Intronix, Bolton, Ontario).

After the P-unit location had been identified (with 20-Hz sine wave stimulation), we used RAM stimuli to characterize the relationship between the stimulus intensity and P-unit discharge rate (f-I relation). The stimulus was generated by multiplying the fish's EOD (MT3; TDT, Alachua, FL) on a cycle-by-cycle basis with the RAM stimulus; its contrast was controlled via a programmable attenuator.

P-type units were identified on the basis of their phase locking to the EOD, skipping response to the baseline EOD, and phase locking to direct stimulation. Once a receptor was tested for phase locking to a global 20-Hz AM stimulus, the same 20-Hz AM stimulus was delivered locally to find the receptor on the surface of the fish. By adjusting the position of these local stimulation electrodes along the head-tail and dorsal-ventral axes of the fish, it was possible to find the location producing a maximal response from the recorded P unit. The local electrodes used to measure the field gradient at the receptor pore were oriented perpendicular to the global stimulation electrodes but, because the fish's body curves appreciably at its dorsal aspect, were not necessarily perpendicular to the skin. Because the effective stimulus for an electroreceptor is the current flow across it (perpendicular to the skin) (Nelson et al. 1997), a correction factor was applied based on measurements of the body curvature; this produced the final estimate of the effective intensity of the stimulus driving the P-unit (average correction: $0.84 \pm 0.17 \times$ measured amplitude).

Action potentials, the EOD, the field gradient, and the attenuated stimulus were digitized at 20 kHz with a 12-bit Multi-IO-board (PCI-MIO-16E-4; National Instruments, Austin, TX) on an Intel Pentium IV 1.8 GHz Linux PC. Spike and EOD detection, stimulus generation and attenuation, and preanalysis of the data were performed on-line during the experiment with our custom software (On-line Electrophysiology Laboratory, created by J. Benda). All data analysis was performed with MATLAB (The Mathworks, Natick, MA).

Estimating the P-unit f-I function

The classic method for constructing f-I curves calculates spike rates in response to step changes in stimulus intensity. The rapid adaptation of P-units to steady-state changes in EOD (Bastian 1981a; Benda et al. 2005; Xu et al. 1996) amplitude precludes this method. Instead we computed f-I curves using two methods adapted from Brenner et al. (2000) using double the cutoff frequencies found during late (~2 Hz) and early (~25 Hz) phases of prey detection (Nelson and MacIver 1999): a Gaussian RAM with a low-frequency cutoff of 4 Hz and a contrast of 5, 10, and 15%. Gaussian RAMs with a 50-Hz cutoff frequency were presented for 180 s at 10% contrast. The former stimulus protocol was repeatedly delivered for 10 s with 2-s rests (frozen noise, 15–100 presentations), and analyzed using counting windows (32 or 64 ms) to generate the spiking rate versus intensity relationship. The latter protocol, analyzed using the covariance method (Brenner et al. 2000), utilized a cutoff frequency that did not exceed the Nyquist frequency for any P unit in our sample (minimum P-unit mean firing rate can be ~100 Hz), which evoked only one or a small number of spikes over the time scale of the fastest fluctuations in the stimulus; further, a 10% contrast stimuli tests for the full coding range up to saturation of the response. Preliminary experiments had shown that the covariance method works best under these conditions and is not optimal for the 4-Hz cut-off stimulus. P-units, because of their high discharge rate, responded throughout the low-frequency stimulus (Fig. 1), and this resulted in gradually decreasing eigenvalues instead of two dominant ones (see following text); in this case the covariance method is not informative.
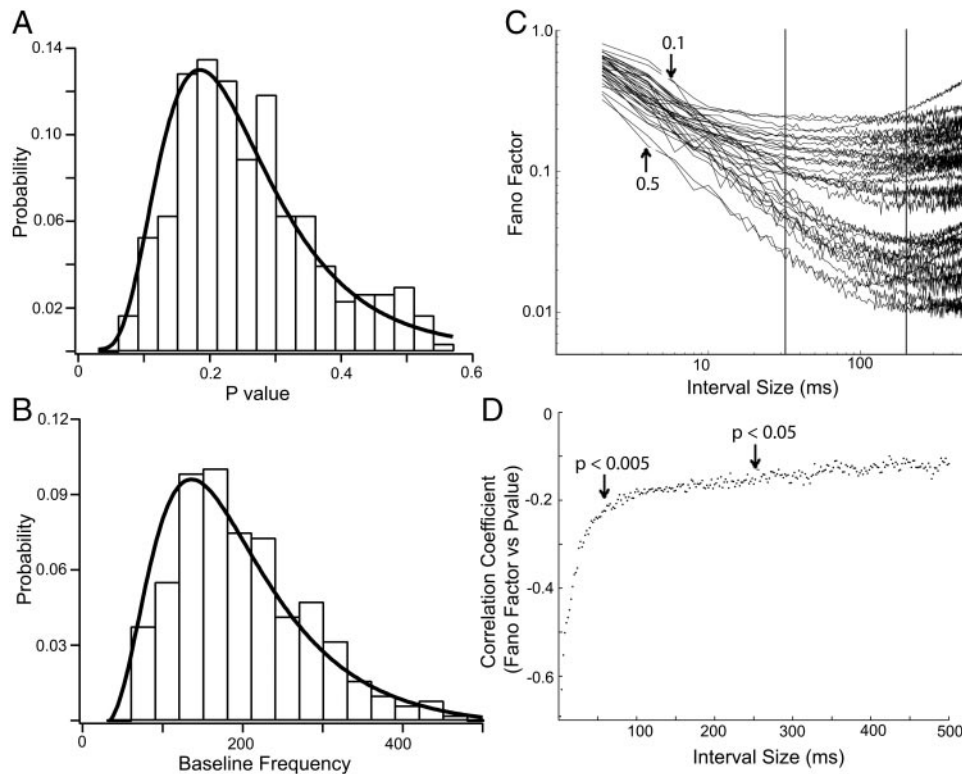
FIG. 1. *A*: *P* value distribution and lognormal fit. The μ and σ values are -1.42 and 0.46, respectively, with a mean of 0.26 ± 0.11. *B*: distribution of P-unit firing rates distribution and lognormal fit. The μ and σ values 5.23 and 0.44, respectively, with a mean of 199 ± 81Hz. *C*: Fano factor curves of a subset of P units. The 2 vertical lines indicate the 32- and 200-ms time points. The arrows identify the *P* values for 2 representative units that demonstrate the lower variance of the high-frequency P units. *D*: correlation coefficient of the *P* value vs. Fano factor for varying counting windows, plotted against the corresponding counting windows. With time intervals <50 ms, there is a very strong inverse correlation between *P* value and the Fano factor ($P < 0.005$). Significant negative correlations persist for counting windows ≤250 ms.

Data analysis

P-UNIT BASELINE ACTIVITY. We routinely computed the interspike interval (ISI) histogram, spike train serial correlations and the Fano factor as previously described (Chacron et al. 2001; Ratnam and Nelson 2000). The Fano factor is the variance to mean ratio of the spike count as a function of the counting interval; we used intervals ranging from 2 to 1,200 ms (absolute time) or 2–1,200 EOD cycles.

LOW-FREQUENCY STIMULATION. A stimulus with a maximum frequency of 4 Hz could, in principle, be sampled at 8 Hz; in practice, such sampling produced noisy f-I curves. We present analysis using 32-ms sampling bins; sampling at 64 ms produced similar results (data not shown), but we use the faster sampling so that our results might be applied to the higher-frequency AMs generated during initial prey detection in these fish (>10 Hz) (Nelson and MacIver 1999). In addition, when given a step change in amplitude, the P-unit spike train is mostly adapted by 30 ms and, in its adapted state, responds linearly to the full range of intensities (Benda et al. 2005).

The corrected field gradient and the spike train response were therefore partitioned into 32-ms bins, overlapping by 16 ms; a 3-ms delay was used between the start of the stimulus window and the start of the spike count window to account for latency/conduction delays (1.6–5.6 ms) (Bastian 1981b). The mean value of the stimulus in each bin was calculated and the mean EOD amplitude (without stimulation) subtracted from this value to give the mean stimulus change from the baseline EOD amplitude; we then computed the relative stimulus as the percent change of stimulus intensity from the baseline EOD amplitude and designate this as %ΔI. This was done to permit comparisons of P-unit responses across fish with differing EOD amplitudes. The mean spike count (unstimulated) or rate was also subtracted from the spike count per window to give the change in count (rate) from baseline; again we also computed the relative spike count or rate by dividing the change in spike count by the baseline count (rate).

Thus we could compute either the absolute or relative change in spike count of a P-unit in response to a relative change in stimulus

intensity. These methods gave different results in some cases and which method is preferable depends on the putative decoding mechanism performed by downstream neurons (see following text).

The spike counts were subsequently analyzed in three ways: the spike count mean and variance were computed across all repeated stimulus presentations for the same 32-ms window; in this case, both the mean stimulus intensity and the stimulus slope are constant for each bin, but the sample size is small—this is termed vertical analysis (vertical divisions of Fig. 2*A*); the spike count mean and variance were computed between amplitude increments of 1 μV across the entire stimulus and the responses to the same mean intensities were grouped together. In this case, the mean intensity within each window remains constant but its slope varies; the sample size is greatly increased. This method is termed horizontal analysis and is based on the assumption that P-units code solely for intensity (Fig. 2*A*); last, we used the second method but separately analyzed the spike counts occurring on up and down slopes of the signal; this is described as the slope-horizontal analysis. (Fig. 2*A*).

The spike count (absolute or relative) was graphed versus the relative intensity change, where the middle 75% of all data points for the 5% contrast stimulus were used to calculate the slope of the line of best fit and the residuals computed. Any residual more than five times the SD outside of the middle 75% data set was excluded in the determination of the coding range of the receptor. The SDs from the differing analyses were compared via ANOVA. The root mean square error (RMSE) was calculated using the line of best fit for all methods of analysis.

HIGH-FREQUENCY STIMULATION. The covariance method, as outlined by de Ruyter van Steveninck (de Ruyter van Steveninck and Bialek 1988) and used to characterize motion-sensitive neurons in the fly (Brenner et al. 2000), retinal ganglion cells (Fairhall et al. 2006), and brain stem auditory neurons (Slee et al. 2005), was used for this analyses. We first computed the reverse correlation, or spike triggered average (STA), for the 20 ms (1-ms bins) preceding each spike; preliminary analysis showed that the STA declines to baseline by 20 ms and that longer time windows do not change the subsequent
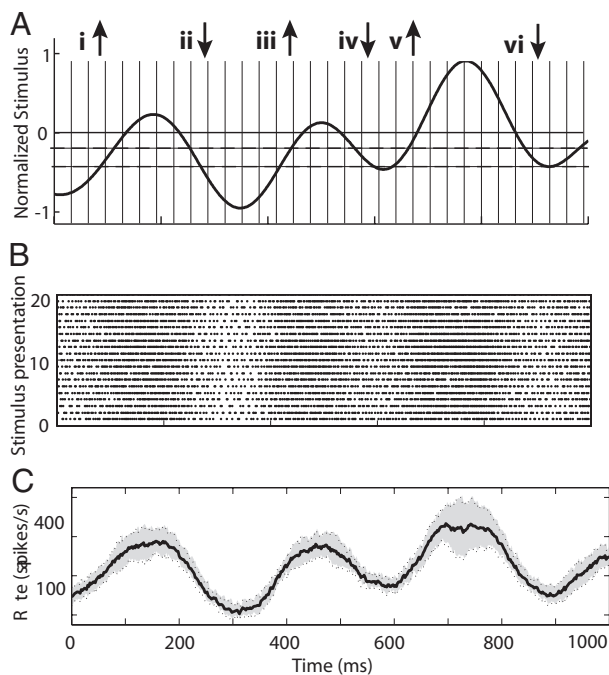
FIG. 2. Overview of stimulation and analysis protocol. *A*: 1-s sample of the global low-frequency Gaussian noise stimulus [0- to 4-Hz random amplitude modulation (RAM), 10% contrast]. Vertical lines demonstrate the discretization into 32-ms time bins; the spike counts down each vertical bin served as the basis for the Vertical analysis. The dashed gray horizontal lines are one slice through the signal; the sections sampled have equal mean intensities but their slopes can vary considerably (e.g., compare ii with iv). Combining all samples (i–vi) served as the basis for the horizontal analysis, whereas separating positively (i, iii, v) and negatively (ii, iv, vi) slope regions served as the basis for sloped-horizontal analysis. *B*: raster plot of a P-unit discharge in response to each stimulus presentation. Spikes are counted in 32-ms bins (vertical) for each presentation. *C*: mean time-dependent firing rate estimated from the raster plot (32-ms bins) overlapped at 2-ms intervals. The firing rate faithfully follows this relatively strong stimulus (10% contrast); we note that these fish are capable of detecting contrasts of <1% (Nelson and MacIver 1997). Gray band represents 1 SD; the increased variability seen at the stimulus peak is due to the near saturation of the response for this unit.

analysis (data not shown). In addition, an equal number of randomly sampled 20-ms vectors were used to compute the mean stimulus independent of the occurrence of spikes. From these mean vectors, we computed the covariance matrix of the STA (C spike in the terminology of Brenner et al. 2000) and the covariance matrix of the random sampling of the stimulus (C prior in the terminology of Brenner et al. 2000). Subtracting these matrices gives the covariance matrix associated with the stimulus induced spikes (ΔC in the terminology of Brenner et al. 2000).

We computed the eigenvalues and eigenvectors from the ΔC matrix. The relative contribution of each eigenvector was assessed by dividing the absolute value of the eigenvalue by the sum of absolute value of all the eigenvalues. Because the two largest eigenvalues (E1 and E2) accounted for 90–95% of the total variance, we confined further analysis to the associated eigenvectors; detailed analysis was carried out only for the eigenvector associated with the largest eigenvalue as discussed in the following text.

We then computed the dot product of each 20-ms stimulus vector preceding a spike onto E1; this projection of the stimulus onto E1 estimates their similarity (S). This can be computed relative to the maximal EOD amplitude (this measure is used in the figures); it can also be computed as an absolute value (μV) because it is merely the E1 weighted mean of the signal. The same computation was carried out for the randomly sampling of 20-ms stimulus vectors. Both sets of projection values were then binned producing a probability densities

defined as the $P(S|\text{spike})$, for prespike stimulus projection values, and $P(S)$ for the random sampling, both of which are related to the relative intensity of the stimulus. Bayes theorem states

$$\frac{P(\text{spike}|S)}{P(\text{spike})} = \frac{P(S|\text{spike})}{P(S)} \qquad (1)$$

where $P(\text{spike})$ is defined as the overall probability of spike discharge per EOD cycle (this is taken during stimulation and is nearly identical to the receptor's P value) and $P(\text{spike}|S)$ is proportional to a normalized rate as a function of the degree of similarity (S) to E1 (as described in Brenner et al. 2000; Slee et al. 2005); we also converted the conditional probability, $P(\text{spike}|S)$, to a firing rate by multiplying it with the EOD frequency. $P(S|\text{spike})$ is readily calculated from the probability density of S (the projection of spike triggered stimuli onto E1). $P(S)$ was calculated from the probability density of the randomly sampled stimuli. An f-I type relation was obtained by plotting the normalized firing rate versus S1 (Fig. 9B). We then carried out the calculations in the preceding text for 20-s segments of the stimulus and computed the mean f-I curve; we then estimated the noise of this f-I curve by computing the SD of the individual f-I curves from the mean. Similar calculations were performed for the projection of the stimuli onto E2; the resulting f-I curves are generally linear with small slopes (data not shown) as expected from the small values of the E2 eigenvalue (see following text). Because we are primarily interested in the response of P-units to stimulus intensity, these results are not further discussed.

RESULTS

We recorded P-unit activity from a total of 54 fish. EOD frequency is highly correlated with the sex of the fish: males typically have EOD frequencies of 800–1,000 Hz, whereas females are between 600 and 800 Hz (Zakon et al. 2002). Because the EOD frequencies of the fish ranged from 630 to 970 Hz with approximately equal numbers more than and <800 Hz (data not shown), we assume that we were sampling from both sexes. No difference in P-unit properties were noted in this population as a function of EOD frequency.

We recorded a total of 310 units for baseline activity (36 fish) with a mean baseline spiking frequency of 199 ± 81 Hz (range of 64–470 Hz); the fish's mean EOD frequency was 782 ± 90 Hz. This translates to a mean P value of 0.26 ± 0.11 (range of 0.06–0.60). Both the P value and baseline frequency distribution were well fit by a log-normal distribution with μ and σ values of −1.42 and 0.46, respectively (P values) and with μ and σ values 5.23 and 0.44, respectively (firing rate; Fig. 1, *A* and *B*); the modes of the distributions were 0.22 (P value) and 180 Hz (the gamma distribution did not produce good fits, data not shown). The majority of P values were between 0.15 and 0.35 (76%).

It is clear that the P value distribution is not Gaussian; although the excellent fit by a lognormal distribution might be coincidental, it is also possible that there is a deeper functional cause. A P-unit is composed of 25–40 receptor cells innervated by a single axon; each cell makes ≥16 synaptic contacts onto the P-unit axon (Bennett 1989). First, we assume that the number of synaptic sites of one receptor that release transmitter during one EOD cycle is a random variable drawn from some (unknown) probability distribution. We also assume that the electroreceptor cells are independent: that is, the number of active synaptic sites at one receptor is uncorrelated with the number of active sites from another receptor for the same EOD cycle. The potential (postsynaptic) in the P unit afferent fiber at

the time of a single EOD is also a random variable, and it determines the P value of the unit. If the postsynaptic potential were proportional to the product of the number of active sites per receptor taken across all receptors, then the resulting P value distribution would be lognormal; if the postsynaptic potential were proportional to the sum of active sites, then a Gaussian distribution of P values would be expected. Detailed biophysical analysis of the tuberous electroreceptors will be required to test these speculative ideas.

Baseline activity

ISI distributions, as well as phase locking to the EOD, were similar to previously reported results (Nelson et al. 1997; Ratnam and Nelson 2000; Xu et al. 1996). We recorded mainly nonbursty P units (71%, similar to:Xu et al. 1996), and because analysis did not reveal any significant differences between bursting and nonbursting afferents, we pooled the results. The first-order serial correlation coefficient (SCC) of the P units was negative with values similar to those previously reported (Ratnam and Nelson 2000); the value of the SCC was weakly negatively correlated to P value ($R^2 = -0.21$, $P < 0.03$).

As previously described (Ratnam and Nelson 2000), P-unit Fano factor curves (variance/mean of the spike count as a function of counting time) decreased to a minimum (0.063 ± 0.053) occurring between 56 and 1,000 ms (mean of 520 ± 277 ms) before increasing (Fig. 1*C*). Neither the counting window for the Fano factor minimum nor its value were related to the afferent's P value (not significant, $P > 0.10$). At short intervals (<50 ms), P value was strongly inversely related to the Fano factor, and significant negative correlations persisted to 250 ms (Fig. 1*D*).

P unit response to low-frequency noise ($f_c = 4$ Hz)

Low-frequency signals were presented to 77 P units (11 fish). The mean spike count per 32 ms appears to faithfully track the stimulus intensity of the 0- to 4-Hz RAM stimulus (comparing Fig. 2, *A* with *C*). Plotting either absolute or relative mean change in spike count versus relative intensity revealed a central linear range, representing the effective coding range of the receptor, bounded by sections of zero-slope and/or irregular spiking indicative of saturation due to very low or high intensities (Fig. 3*A*).

Linear fits were initially performed to the central region (using 75% of the data surrounding the baseline spike count) and then extrapolated outward. Very good linear fits were achieved for all P units ($R^2 = 0.94 \pm 0.14$, $P < 0.005$). The residuals (Fig. 3*B*) calculated from the linear fit were then used to define the lower and upper limits for linear coding for each P unit: residuals outside of the central region and larger than four times the central residual SD were excluded. The linear coding range of these neurons is independent of P value and stimulus contrast (the minimum and maximum intensities are -17 ± 7.5 and $17 \pm 8.8\%$, respectively) of the baseline EOD amplitude; spiking is silenced at the low intensities and saturated at approximately double the baseline firing rate. The SD did not change significantly over the entire coding range (Figs. 3*A* and 6*A*). This coding range is sufficient to encompass the full intensity range of low-frequency signals expected during electrolocation (Babineau et al. 2006; Chen et al. 2005).
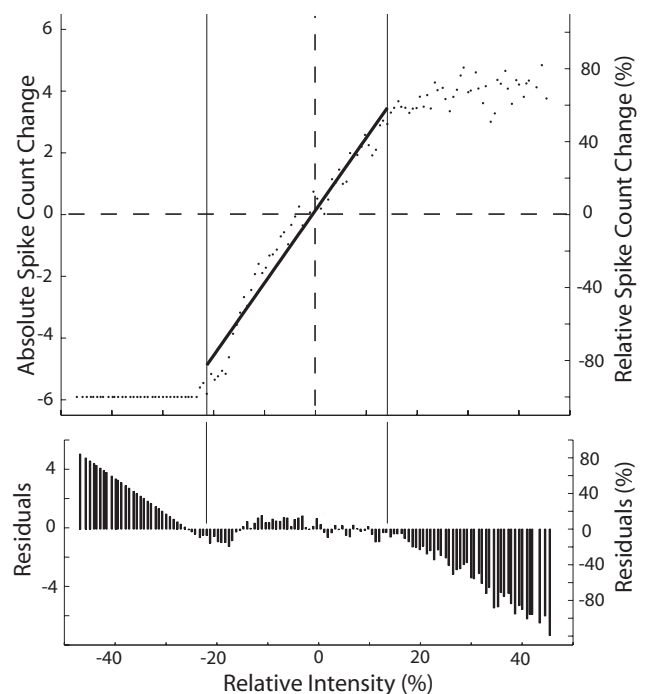

FIG. 3. *A*: f-I plot. The mean change in spike count within 32 ms is plotted against the relative change of stimulus intensity (10% contrast); a linear fit to the central region (thick solid line) was used to compute P-unit gain (slope) and range. The coding range of this unit is indicated by the thin vertical lines. *B*: residuals of the fit when extended over the entire stimulus range.

Gain is positively related with P value when absolute spike counts are used (range: 0.035–0.447 spike·32 ms^{-1}·%ΔI^{-1}, avg. gain $= 0.197$ spike·32 ms^{-1}·%ΔI^{-1}, $R^2 = 0.55$ where $P < 0.01$; Fig. 4*A*). Following the convention in this field, we convert the rate to spike/s (Fig. 4*A*; range: 1.1–14.0 spike·s^{-1}·%ΔI^{-1},[r] mean gain $= 6.16$ spike·s^{-1}·%ΔI^{-1}). This suggests that if target pyramidal cells in the electrosensory lateral line lobe (ELL) can detect absolute changes (± 1 spike/s) in the P-unit spike count, then high P value receptors will be most sensitive to small changes in intensity. As noted in METHODS, percent changes in intensity were used to compare between fish with varying EOD amplitudes. We repeated these calculations for absolute (μV) changes in intensity: for a 1-μV/cm change (averaged over 32 ms), we expect (averaged across all P values) an extra 0.32 ± 0.17 spike/s. This value is lower than the ~ 1 extra spike/s per μV/cm given in earlier reports (Bastian 1981a; Nelson et al. 1997). It is possible that by extrapolating the gain-frequency relationship down from minimum experimental intensities of 63 μV/cm (Bastian 1981a) and 10 μV/cm (Nelson et al. 1997), gain at 1 μV/cm is overestimated. The discrepancy might also, in part, be due to differences in methodology: Bastian used SAMs (as opposed to RAMs) with large increases in intensity and extrapolated down to microvolt levels. Nelson based his estimates on the use of sinusoidal amplitude modulations and P-unit models that were in turn calibrated by Bastian's earlier data. This disparity strongly affects the number of downstream neurons required to detect small changes in input; we further discuss this discrepancy after describing the results of our covariance analysis in the following text (also see DISCUSSION).

The relative spike count per relative intensity (i.e., relative gain) has no relationship to the baseline spiking frequency or P
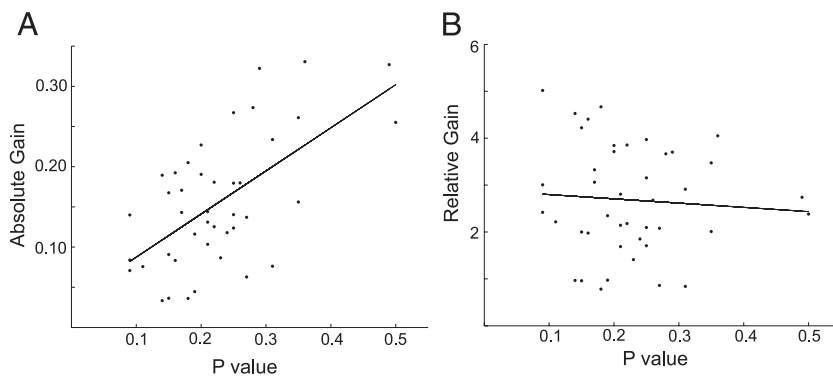
FIG. 4. Gain vs. *P* value. *A*: when absolute spike count within 32 ms are used, the gain of a P unit is positively correlated with its *P* value: $R^2 = 0.59$ at 5% contrast stimulation ($P < 0.001$), $R^2 = 0.67$ at 10% contrast stimulation ($P < 0.001$). *B*: for relative spike counts, the gain is independent of *P* value.

value (range: 0.76–8.01%spike/%ΔI; Fig. 4*B*). A relative measure would be appropriate if downstream neurons normalized the P-unit baseline input by, for example, synaptic depression (Abbott et al. 1997). Because this possibility is entirely speculative, we follow previous authors (Bastian 1981a; Nelson et al. 1997) and present results solely as absolute spike count and spike rate.

P-units show strong adaptation to sustained or slowly changing input (Benda et al. 2005; Nelson et al. 1997; Xu et al. 1996), implying that the extent of adaptation might be different on the positive and negative slope of the stimulus waveform and contribute to the variability of the P-unit response. We therefore computed the f-I curves independently for the positive and negative slopes of the stimulus (sloped-horizontal analysis, Fig. 5). The coding range and the defined maximum and minimum firing frequencies were the same regardless of the sign of the stimulus slope and were not significantly different from those values computed for the entire stimulus and across various stimulus contrasts.

The gain of the f-I curves was the same for horizontal and sloped-horizontal curve analyses. However, the curve generated from the positive slope sections of the stimulus was leftward displaced in comparison with the curve from the negative slope sections while the negative slope sections were rightward displaced (8.5 ± 4.5% intensity difference; black bar, Fig. 5); the linear fit for the horizontal analysis was located symmetrically between these curves (data not shown). This result is consistent with the dynamics of P-unit adaptation because the firing rate is low at the onset of the positive slope, reducing adaptation and therefore causing a shift of the neuron's f-I curve to lower intensities (Benda and Herz 2003). This result implies that a linear rate code estimate of signal intensity will be biased if the gain for the horizontal analysis is solely used in its computation (Fig. 3*A*).

As observed for the curves generated from the horizontal analysis, the SD (noise) for the sloped-horizontal curves remained constant over the entire linear coding range. However, the noise for the horizontal curve is greater, over the entire linear coding range, than that of the sloped-horizontal F-I curve (Fig. 6, *A* and *C*). Under the assumption that the SD reflects P-unit noise, this implies that noise levels will be reduced if a central decoder could separate P-unit spikes emitted during the positive versus negative slopes of the stimulus. This idea was further investigated by computing the spike count variability around the mean of the baseline discharge in response to varying levels of contrast. This spike count distribution (for all conditions) can be well approximated as Gaussian (Fig. 6*B*),

and we have previously noted that the spontaneous variability might represent noise because it occurs independent of stimulation (Chacron et al. 2001). The SD of the spike count computed vertically (no variation in stimulus slope) was not significantly different from that of baseline variability [0.71 ± 0.18 spike/32 ms (22.16 ± 5.5 spike/s) vs. 0.68 ± 0.18 spike/32 ms (21.33 ± 5.5 spike/s), Fig. 6*C*].

In contrast, the horizontally computed variance was significantly higher and increased with the contrast (as previously reported by Wessel et al. 1996): at 5% contrast, horizontal noise [0.91 ± 0.33 spike/32 ms (28.40 ± 10.4 spike/s), $P < 0.001$] is 40% greater than the vertical noise and increases by 40% for each 5% increase in contrast. Furthermore, the contrast for the total stimulus was, at any contrast, greater than that computed for positive and negative slope: the sloped-horizontal noise [0.74 ± 0.21 spike/32 ms (23.03 ± 6.5 spike/s)] is only 18% greater than the vertical noise and increases 18% for each 5% increase in contrast. Similar results were obtained when absolute or relative spike counts were used (data not shown).

Because an increase in contrast will increase the variability in stimulus slope, this data suggests that at least a portion of the "noise" may be due to the P unit responding to variations in stimulus slope. By separating the stimulus into increasing and decreasing changes in amplitude, the variability is reduced
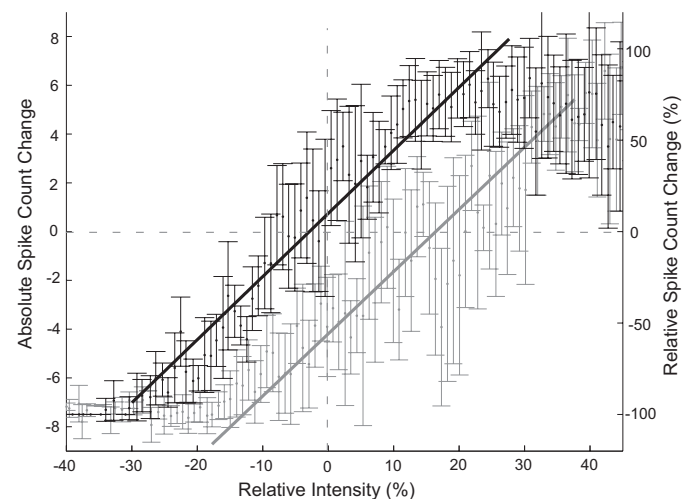

FIG. 5. f-I curves for positive (black line) and negative (gray line) stimulus slopes with error bars (SD) and best fit lines (solid and dashed, respectively). f-I gain is the same for both slopes but there is an offset by a spike count bias; the f-I curve for the entire data set shown in Fig. 3 would lie precisely in the middle of these curves. The intensity range (ends of best fit lines) are equal and independent of baseline *P* value.
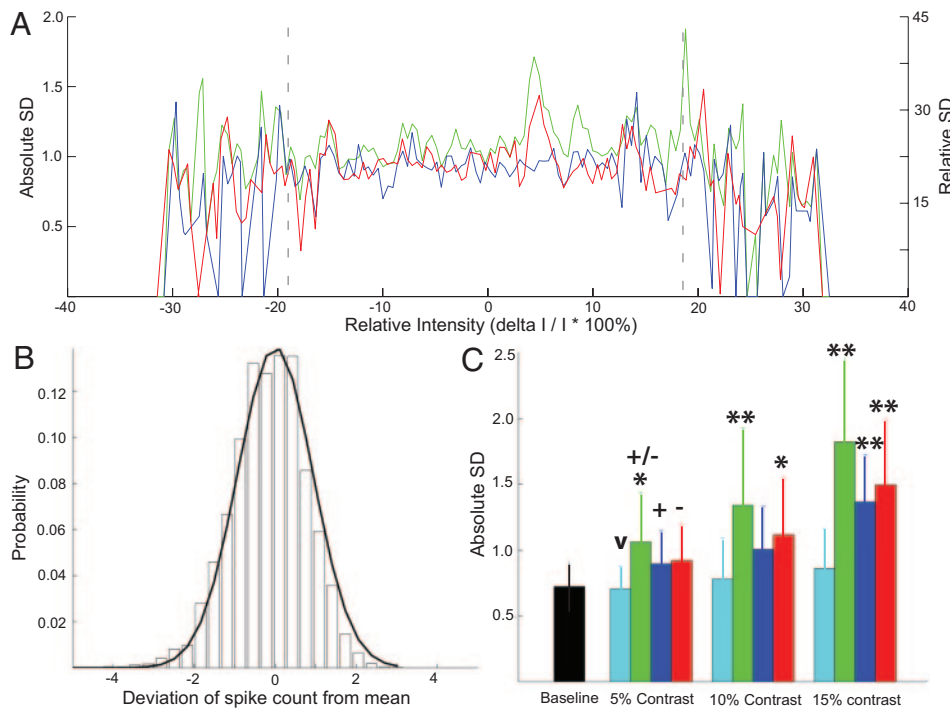
FIG. 6. *A*: SD of the spike count (within 32ms) over the coding range for counts pooled over the entire stimulus (green) vs. separate counts for the positive (blue) and negative (red) slopes of the stimulus. The SD becomes more variable outside the coding range (dashed gray vertical lines) because of either erratic discharge or saturation effects. Note that the SD of the spike counts for both the positive and negative slopes are typically lower than those for the entire stimulus. *B*: spike count distribution of stimulated discharge for 32 ms (mean subtracted) of a typical P unit averaged across all bins (vertical analysis, 5% contrast). Black line is the Gaussian fit to this data. *C*: SD of the absolute spike count within 32 ms for baseline discharge (black), vertical (v, light blue), horizontal (±, green), positive stimulus slope (+, blue) and negative stimulus slope (−, red) for contrasts ranging from 5 to 15%. Significance is based on comparisons with the vertical SD within a given contrast, with 1 star ≡ $P < 0.05$ and 2 stars ≡ $P < 0.01$ (ANOVA). The vertical SD is not significantly different from that of the spontaneous discharge at all contrasts. The results are similar for the relative spike count.

compared with horizontally computed noise. In fact, in the limit of the very low contrasts that occur during prey detection (<2%) (Nelson and MacIver 1999), additive Gaussian noise is equal to the variance of the baseline spike count [even at 5% contrast, vertical noise: 0.71 ± 0.18 spike/32 ms (22.16 ± 5.5 spike/s) and sloped noise: 0.74 ± 0.21 spike/32 ms (23.03 ± 6.5 spike/s) were not significantly different from baseline variability (0.68 ± 0.18 spike/32 ms (21.33 ± 5.5 spike/s)]; variability of baseline discharge is therefore a valid approximation of the noise in rate coding models of the P-unit response to weak low-frequency signals.

The effect of eliminating the bias and reducing the variance can be assessed from the accuracy of stimulus reconstructions based on the computed linear f-I curves. When reconstructing the stimulus using the 5% contrast gain (to avoid the saturating regions), the mean square error between the original stimulus and its reconstruction is reduced more than threefold when positive/negative slope are taken into account (absolute spike count: total RMSE = 9.37 ± 4.74 μV; sloped RMSE = 2.86 ± 0.80 μV); similar results were obtained when using the relative spike count (data not shown).

F_c = 50-Hz stimulus-response characteristics

The 0- to 50-Hz signals were presented to 45 P-units (7 fish). Our analysis suggested that the P units were responding to both the intensity and slope of the low-frequency RAM signals; we therefore turned to a recently developed method that can explicitly decompose the spiking response of a neuron to a linear combination of time-dependent vectors. We used the covariance method of de Ruyter van Steveninck et al. (1988) and Brenner et al. (2000) with high-frequency RAMs (50-Hz cutoff) as stimuli. We first computed the STA; this vector is positive just preceding a spike and rapidly drops to negative value before settling to 0 (baseline EOD amplitude) by 20 ms (Fig. 7A), as previously reported in earlier studies of a related

electric fish (Wessel et al. 1996). The shape of the STA and its spectrum are independent of EOD frequency and *P* value (data not shown). We also used the STA (corrected for the autocorrelation/power spectrum of the spike train) (Gabbiani 1996; Wessel et al. 1996) to evaluate the error of linear signal reconstruction; we found coding fraction values (range cf. = 0.640–0.925, mean cf. = 0.798 ± 0.089) consistent with earlier studies on a related electric fish (Wessel et al. 1996).

The eigenvector (E1), corresponding to the largest eigenvalue of the spike-triggered covariance matrix, was very similar to the STA (Fig. 7A). The STA, and therefore E1, represents the time-weighted intensity—positive for ~6 ms preceding a spike and negative back to ~20 ms—of the stimulus that is likely to evoke P-unit spiking and accounts for most of the variance of the response (65–85%) for all *P* values. The second eigenvector (E2), corresponding to the second highest eigenvalue, resembles the derivative of the STA and is therefore a measure of the local slope or change of the stimulus (Fig. 7A).

The relative contribution of the covariance matrix eigenvalues to the total variance drops rapidly and, as reported in other sensory systems (Brenner et al. 2000; Slee et al. 2005), the first two eigenvalues account for, on average, 92% percent of the total variance (85–95%; Fig. 7B). Similar results were obtained when 0- to 100-Hz RAMs were used (data not shown).

The relative contribution of the first and second eigenvalue varied systematically with *P* value so that higher *P* value receptors tend to have a stronger E1 contribution, whereas those with low *P* values have a larger contribution from the second eigenvector (though still less than E1, and E2 drops to almost 0 at higher *P* values; $R^2 = 0.52$, $P < 0.02$, Fig. 8). This suggests that low *P* value receptors are better suited to signal changes of intensity, whereas high *P* value receptors can code almost entirely for the first eigenvector (intensity). Because E1 is closest to the "intensity" variable of f-I curves, our subsequent analysis is focused on the E1 vector. The contribution of
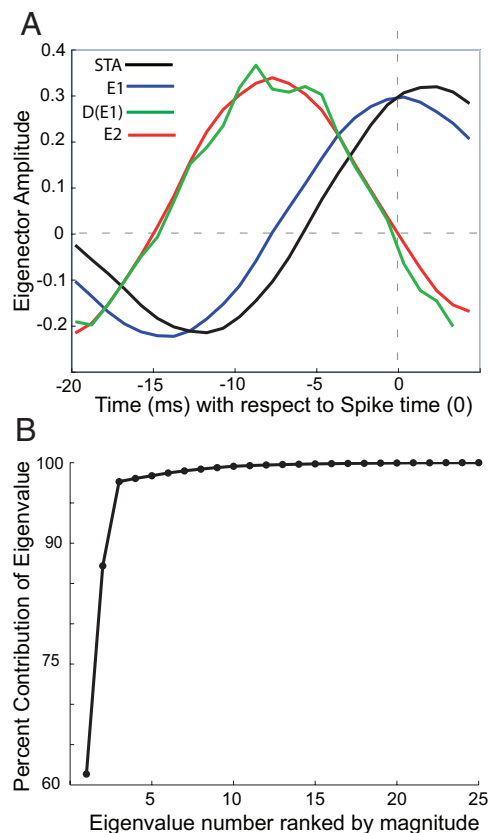
FIG. 7. *A*: The spike-triggered average (STA, black) is nearly identical to the 1st eigenvector (E1, blue); the 2nd eigenvector (E2, green) resembles the derivative of the E1 (red). The STA decays to 0 by 20 ms and no change in E1 or E2 was seen when STA was calculated for longer prespike intervals. *B*: cumulative percent strength of the eigenvalues. The 1st and 2nd eigenvalues account for ~87% of the variance in the response for this P unit.

average minimum and maximum values of –17.99 ± 10.7 and 18.85 ± 10.6% similar to those for 4-Hz stimulus. As previously described for f-I curves derived from 4-Hz stimuli, the P unit is silenced at the lowest S values (when the signal is most dissimilar to E1) and is approximately double the baseline firing rate at the upper end of the coding range. The maximum normalized rate therefore increases with baseline frequency ($R^2 = 0.65$, $P < 0.005$). Neither the normalized relative intensity (S) range, nor the normalized gain (range: 2.84–13.02 spike·s^{-1}·%ΔI^{-1}, avg. 5.76 ± 3.04 spike·s^{-1}·%ΔI^{-1}) were related to the P-unit baseline frequency. Further, both intensity range and normalized gain are similar to the 4-Hz gain data, suggesting that the Brenner et al. method produces f-I curves comparable to those calculated with low-frequency RAMs and the counting window method.

We therefore attempted to calculate the absolute gain of this f-I curve: the increase in spike count to a 1-μV/cm increase in stimulus intensity from the S projection values. A 1-μV change in intensity causes a 2.38 ± 1.09 spike·s^{-1}·μV^{-1} change in firing rate or a 7.3-fold increase over the 4-Hz gain. Earlier studies have also shown that gain increases with frequency (Bastian 1981a) but estimate a slightly lower (~5- to 6-fold) increase in going from 4 to 50 Hz (Chacron et al. 2005a; Nelson et al. 1997).

Benda et al. (2005) computed the f-I curves at both the onset of step changes in EOD amplitude (f_0) and after adaptation (f_∞). Both f_∞ and f_0 are linear with slopes of 0.32 spike·s^{-1}·μV^{-1} (this paper: 0.32 spike/s/μV) and 1.97 Hz/μV (this paper: 2.38 spike·s^{-1}·μV^{-1}), respectively (these were computed from the data published in Benda et al. 2005) giving a sixfold increase. Our low-frequency (4 Hz) signals are similar to the f_∞ condition with respect to the state of adaptation of the P-units; similarly, our 50-Hz stimuli are similar to the f_0 condition. It is therefore not surprising that the Benda et al. estimates are also very similar to those calculated for our low- and high-frequency stimuli, although again we have estimated slightly higher gain for the 50-Hz RAMs. Our low estimates for mean low-frequency gain might therefore be more accurate than previously reported values. However, all estimates of the relative frequency dependence of gain are in approximate agreement. Both the method employed in this paper and that of

E1 to the variance (mean = 76%) is similar to the stimulus-response coherence of P units (60–80% for frequencies ≤50 Hz) (Chacron et al. 2005a). These are linear methods and both rely on the cross-correlation of stimulus and evoked spike train. Although subsequent data analysis is different (covariance matrix decomposition versus Fourier transform to the frequency domain) it is reassuring that they nonetheless give comparable results.

Projecting the prespike vectors onto E1 computes its similarity to E1 and thus to the time-weighted intensity; we designate this value as the normalized relative intensity (S). Estimating the probability of a spike given the occurrence of E1 provides a measure of the spike rate. These quantities are connected via Bayes theorem and, as previously described (Brenner et al. 2000), were used to compute a normalized f-I curve by plotting the normalized firing rate versus the normalized relative intensity (see METHODS). To estimate the noise remaining in this derived f-I curve, we computed the f-I relation for 20-s segments of the recordings and calculated the SD of the curve from the variations of individual curves with respect to the mean curve.

Plotting S1 versus the normalized relative intensity generates a linear relationship (Fig. 9). This linear region is bounded by regions of saturation or highly variable spiking similar to the results for the $f_c = 4$-Hz stimulus, defined by the largest region where the mean normalized spike count exceeds the noise. The normalized relative intensity coding range has
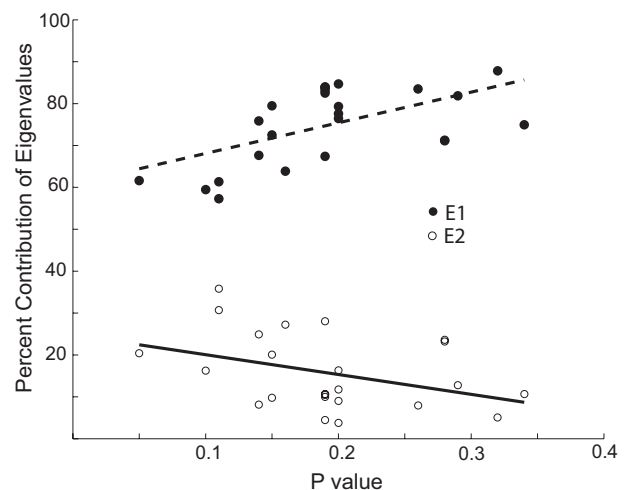

FIG. 8. Relative contribution of the E1 (● and E2 (○) eigenvalues to total variance as a function of P value. E1 increases with P value, whereas E2 decreases. The sum of E1 and E2 is constant at 90–95% across all P values (not shown).
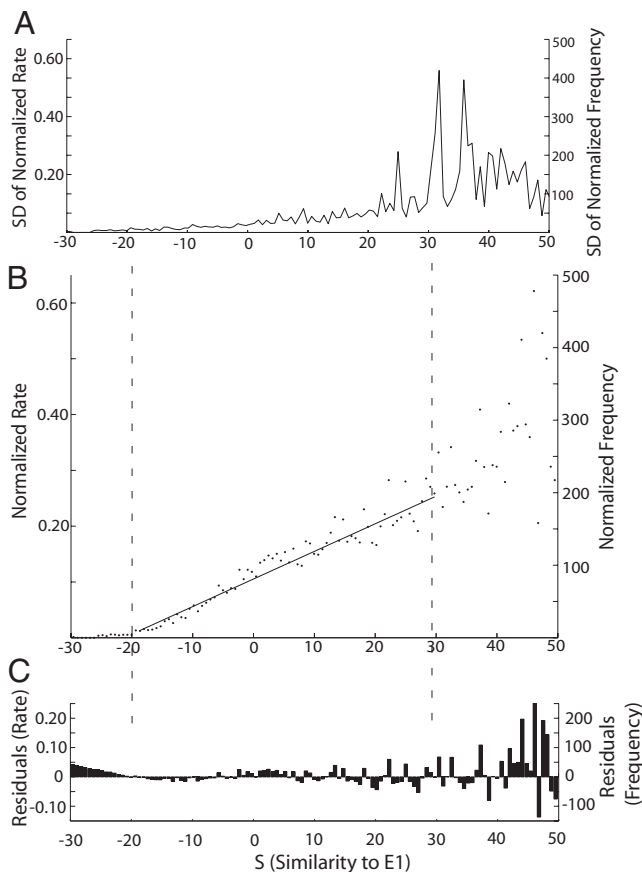
FIG. 9. *A*: SD of normalized f-I plot derived by creating 9 equal-sized time segments, calculating the normalized rate within each and the SD between them. *B*: normalized f-I curve showing the relation between normalized firing rate to the similarity of the stimulus to E1. —, linear fit within the coding range, defined as the region between saturation and when the SD is larger than the firing rate. *C*: residuals from the linear fit.

Benda et al. (2005) showed a large variability in the gain of individual P units. It is therefore also possible that the P-unit population can fractionate the large intensity range of electrosensory signals; although this might, in principle, improve coding for both strong and weak signals, it would also mean that a decoder might not be able to utilize simple averaging over the entire population. We do not therefore consider this more complicated possibility in the following text.

The SD of the normalized firing rate increases with the value of S ($R^2 = 0.49$, $P < 0.001$), ranging from 15 to 65% of the normalized firing rate. This is likely due to undersampling—there are few samples for high values of S that makes the values of $P(S)$ very small and variable; because $P(S)$ is used in the denominator (*Eq. 1*), this variability becomes magnified. For small natural electrolocation signals (within 2% of baseline EOD amplitude) (Nelson and MacIver 1999) appropriate to the detection of prey items, the SD is 22.37 ± 4.04 spike/s. This value is nearly identical to the SD of the baseline spike count (over 32 ms), suggesting that noise due to baseline variability of P-unit discharge is the final limit for rate coding in the electrosensory system.

DISCUSSION

The coding of time varying signals by P-unit electroreceptors of high-frequency wave type electric fish has been the subject of numerous investigations (Bastian 1981a; Benda et al. 2005, 2006; Chacron et al. 2001, 2005a; Kreiman et al. 2000; Ludtke and Nelson 2006; Nelson et al. 1997; Ratnam and Nelson 2000; Wessel et al. 1996; Xu et al. 1996). Although different types of analysis have been used, the overall conclusion is that P -units are good linear encoders over a wide frequency range and that their gain increases with frequency. In *Eigenmannia*, calculation of the optimal STA was used to compute the percentage of the signal variance captured by the P-unit discharge (coding fraction) and coding fractions ≤0.80 have been reported (Wessel et al. 1996). In *A. leptorhynchus*, coherence has been used to demonstrate that linear encoding by P units can capture ~70% of the signal variability over a wide frequency range (Chacron et al. 2005a); further, Chacron (2006) compared stimulus-response to response-response coherence to conclude that little additional information could be extracted by a nonlinear filter.

We have used a more traditional approach, the construction of f-I curves, to confirm that P units are linear encoders; further, the variance of the spike count response was independent of the stimulus intensity, suggesting that an additive noise model is suitable. The advantage of this approach is that it can be immediately linked to a simple putative decoding mechanism: pyramidal cell targets can integrate the numerous P-unit inputs over a time window appropriate to the maximal signal frequency. For the sensory input expected during the fish's prey capture behavior (Nelson and MacIver 1999), integration times of 25–200 ms would be appropriate. Because the response of P units is statistically independent for both baseline and low-frequency input (Benda et al. 2006; Chacron et al. 2005a), the input noise will scale as the square root of the number of P units converging onto a pyramidal cell (see following text).

f-I curves are often constructed using constant inputs; we have used the Brenner et al. (2000) method for slowly varying input appropriate to the frequencies expected in the final phases of prey capture (4-Hz cutoff frequency). We find that the variance and bias of the response are highly dependent on variations in the slope of the signal. This is not surprising because the P unit's high-pass filter response with a cutoff frequency at 1 Hz as described by Nelson et al. (1997) makes them sensitive to the slope of the stimulus in addition to the stimulus intensity. A lower bound on the variance of the P-unit spike count is set by the variance of the baseline discharge (Chacron et al. 2001) and depends on the length of the counting window (Fig. 1) (Nelson et al. 1997). For weak perturbations (<5% contrast as expected for prey) (Nelson and MacIver 1999), the spike count variance approaches this lower bound only if computed separately for responses to the positive and negative slopes of the signal. Separating the response to positive and negative slopes also eliminates a small bias in the response and, together with the reduced variability, leads to far better stimulus estimation. Although separating the stimulus into regions of positive and negative slope is a nonlinear operation, it is performed automatically by the circuitry of the ELL; ELL pyramidal cells can be divided into two major classes—basilar and nonbasilar pyramidal cells (Maler 1979; Maler et al. 1981; Saunders and Bastian 1984). Basilar pyramidal cells (E cells) respond on the stimulus upstroke while nonbasilar pyramidal cells (I cells) respond on the downstroke (Heiligenberg and Partridge 1981).

Weak signal detection

Behavioral experiments have demonstrated that *A. lepto-rhynchus* can detect signals <1 μV and perhaps as low as 0.2 μV (Bastian 1981a; Knudsen 1974; Nelson and MacIver 1999); to assess how well a simple linear rate coding P-unit model performed, we assessed its ability to discriminate 1-μV changes in stimulus intensity. We used the discriminant ($d' = |R_1 - R_2|$/SD), where $R_{1,2}$ are the spike count (SC) at 0 and 1 μV, respectively, and SD the SD of the spike count (Dayan and Abbott 2001) as a ratio measure of neuronal sensitivity to inherent noise. Using the mean 4-Hz horizontal gain, 1 μV produces a mean change of 0.32 $\pm$ 0.17 spike/s, and the mean sloped horizontal SD is 23.03 $\pm$ 6.5 spike/s. By calculating the ΔSC/SD ratio for each neuron individually, the average ratio is 0.0108 $\pm$ 0.0213. Because P units are independent (Benda et al. 2006; Chacron et al. 2005a), the SD will decrease with the square root of the number of neurons; therefore a fish needs $\sim$10,700 P units to accurately detect 1 μV, a number greater than the number of tuberous receptors on one side of the body (7,000–8,000) (Carr et al. 1982).

These fish can take $\leq$200 ms to scan past a prey item, and previous research has assumed that this is the integration time for detection (Ratnam and Nelson 2000). Because our stimulus was a 4-Hz RAM, we cannot directly estimate d' for such long stimuli. We assume, for the weak perturbations used, that both the spike count and its SD would scale with the counting time window in the same way as for baseline activity (as per the Fano factor plot in Fig. 1). In this case, the spike count would increase sixfold, whereas the SD would double when the window went from 32 to 200 ms. This would result in a threefold increase in d' and, consequently a ninefold decrease in the number of neurons to $\sim$1,190. This level of convergence does in fact occur in the lateral segment of the ELL (Maler, unpublished observations). However, although the simple f-I curve might explain the detection of a 1-μV change, it cannot explain detection levels of $\sim$0.2 μV.

The statistical structure of the P-unit spike train is highly constrained by adaptation that decays over many EOD cycles (Chacron et al. 2001; Ratnam and Nelson 2000). Recent studies (Goense and Ratnam 2003; Kreiman et al. 2000) have demonstrated that single extra spikes inserted into a P-unit spike train might be readily detected with few false alarms. If the decoder used by these authors could be scaled up to a large population of P units, then the system sensitivity might be sufficient to detect <1-μV signals; it is not clear whether simple averaging would work, however, because it would require the "extra" spikes be added to all P units at roughly the same time, and it is therefore not clear how such a population decoder would operate. An additional source of information for detecting prey items might be ampullary input but even this might not be sufficient (MacIver et al. 2001). A recent paper (Ludtke and Nelson 2006) has suggested that an optimal estimator operating over the electroreceptor population could use P-unit ISI correlations to greatly improve detection of weak signals; this information is eliminated when rate coding f-I curves are used. The requirement for this method to work was the estimation of conditional probabilities by the dynamics of short term plasticity of P-unit synapses; there is, as yet, no experimental verification of this interesting possibility.

Our results from the covariance analysis of the P-unit response to high-frequency stimuli (cutoff frequency: 50 Hz) suggest another potential mechanism by which the electrosensory system might detect such weak signals. If the electrosensory decoder could extract the first eigenvector from a P-unit spike train response, then it would encode a 1-μV increase with, on average, an extra $\sim$2–3 spike/s with a SD of $\sim$22 spike/s. This reduces the number of P units needed to detect 1-μV fluctuations around baseline EOD amplitude to only $\sim$200 neurons (calculated for each unit and then averaged across units). In this case, even the detection of 0.2 μV would be possible for the lateral segment of the ELL because convergence ratios of 1,000 are seen in this map (Maler, unpublished data).

Note that the high-frequency stimuli necessary for the covariance method probe the P-unit input-output relation in a different frequency band than the low-frequency stimuli used for constructing f-I curves. As a consequence, these two complementary methods reveal signal transmission properties due to different mechanisms. Nelson et al. (1997) characterized the gain of the P-unit's transfer function with two high-pass filters. The first filter had a cut-off frequency at $\sim$25 Hz. This filter is due to rapid spike frequency adaptation as described in Benda et al. (2005), and this filter gives rise to the E1 and E2 components obtained from the covariance analysis of the spike response to high-frequency stimuli. The second filer had a cutoff frequency of $\sim$1 Hz, and it is this filter that causes the f-I curve computed from the response to the low-frequency stimuli to vary with the slope of the stimulus.

The covariance analysis we performed on low level electroreceptor responses is similar to previous studies of low level filtering by visual (Brenner et al. 2000) and auditory (Slee et al. 2005) neurons and reaches remarkably similar conclusions; a recent study has also reported similar results for a subset of retinal ganglion cells (Fairhall et al. 2006). First, there are two dominant filters (eigenvectors): E1 is a smoothing filter (for velocity or intensity) operating over a short time range and resembling the STA; E2 is approximately the time derivative of the first eigenvector and therefore responds to rapid changes of the stimulus. Second, parsing the input with these filters reduces the response variability and/or increases the information transmitted. This is intuitively clear since, as already noted by Brenner et al., much of the "noise" in standard f-I curves comes from the fact that many sensory neurons respond to both the intensity (velocity in their case) of a signal and the change of intensity (acceleration in their case). These stimulus attributes are confounded in classic f-I curves. Therefore low level sensory processing would be far more efficient if downstream decoders could do an eigenvector decomposition of their input. Earlier studies using the covariance method did not address the nature of such putative decoders.

In the case of the electrosensory system, we propose a tentative decoding scheme. P units terminate in the ELL on a number of target neurons including deep and superficial pyramidal cells (PC cells, both E and I types). The deep PC cells respond in a tonic manner to the input signal over a wide range of frequencies (they are receptor-like) (Bastian and Courtright 1991; Bastian et al. 2002; Chacron 2006; Chacron et al. 2005a,b). In contrast, superficial PC cells respond in a phasic manner to the stimulus onset (Bastian and Courtright 1991) presumably because of inhibitory inputs lacking in deep PC

cells (Bastian et al. 2002; Maler and Mugnaini 1994). We propose that superficial PC cells respond to the derivative of the stimulus, whereas deep PCs respond to both the time weighted amplitude and its change. Further, we propose that midbrain neurons downstream of ELL (torus semicircularis, TS) that receive input from both deep and superficial PC cells (Bastian et al. 2004) might subtract the superficial PC cell response from that of the deep PC cell; if the response of the deep PC cell represents E1+E2 and the superficial PC cell E2 alone, then this operation would recover E1. Although this proposal is speculative, future recording in TS should be able to confirm or refute it.

There are two constraints on this scenario. First for very-low-frequency input (<2 Hz), both the STA and E1 become "time-smeared" due to the multiple P-unit spikes per time scale of the signal (data not shown) thus invalidating the covariance method; in this case, the gain is reduced because of adaptation, and the long detection times used (200 ms) encourage a rate coding approach. Second, for very-high-frequency stimuli due to electrocommunication signals, P-units synchronize (Benda et al. 2006) and averaging over P units may no longer be effective; further, the low-pass nature of I cells (Chacron 2006; Chacron et al. 2005b) means that separation by stimulus slope is no longer possible. Thus for high-frequency or transient electrocommunication signals, entirely different temporal coding strategies might be operative (Benda et al. 2006). Given these constraints and following the studies of prey capture by a closely related electric fish by Nelson and colleagues (Nelson and MacIver 1999), we therefore propose the following plausible sensory coding strategy. *Apteronotus* will scan for prey at velocities (>10 cm/s) producing stimulus bandwidths ~20–30 Hz; stimulus intensities at the moment of detection are often weak, <1 μV for prey >2 cm away (Babineau et al. 2006; Bastian 1981a; Chen et al. 2005; Nelson and MacIver 1999). For these frequencies, there is minimal synchronization of P units, and we propose that detecting such weak signals requires estimating E1 over a large number of receptors (lateral segment of ELL) and a short period of time (<50 ms). As the fish approaches the prey, its velocity decreases (<1 cm/s), and the stimulus bandwidth accordingly decreases to <2 Hz. However, the fish is also much closer to the prey (<1 cm); given the rapid drop off of stimulus intensity with distance, this implies much stronger signals (>10 μV). At this point, the eigenvector decomposition no longer works because the signal's frequency is too low. However, the fish, by separating the signals into positive and negative slope (via E and I PC cells), can use simple integration of P-unit input, i.e., the f_∞ or, equivalently, the 4-Hz f-I curve, to estimate the stimulus strength. For such strong, slow signals there can be averaging over a much longer time window (~200 ms), and there need not be extensive spatial averaging (~100 P units would be sufficient to detect 10 μV), and PC cells in the different ELL segments might then provide the spatially high resolution estimate of the prey's exact 3-D location (Lewis and Maler 2001).

Conclusions

First, P units can be simply modeled as independent linear rate coders with additive noise. The amount of this noise can be estimated from the variability of baseline P-unit discharge. P units respond to the rate of change (slope) of signals as well as their intensity; the slope dependent changes in firing, mostly those associated with the rising versus falling slopes, are considered as noise sources in this simple model. A nonlinear operation is therefore required to improve the rate coder: the response to up- versus downstrokes of the signal must be separated by the decoder. This separation is an automatic consequence of the ELL circuitry because E and I cells encode the up- and downstrokes, respectively. For the relatively strong (>5 μV) low-frequency signals that occur during the late phases of prey capture (fish moving at <2 cm/s and prey within <1 cm), this encoding model is adequate. Further, decoding in this case might simply be done by target (pyramidal) cell temporal integration (averaging) of the synaptic input from a moderate number of receptors.

Second, this model is not adequate for the temporal bandwidth of signals present when the fish first detect prey (0->20 Hz and <1 μV). Because the f-I curve is one dimensional, the response of the P units to the strongly varying stimulus slope becomes an additional noise source and this overwhelms the increased gain of the receptors at higher frequencies. In this case, the fish might perform an eigenvector decomposition so as to estimate the signal intensity independent of its slope; this method will permit the detection of such weak signals because, again, a biologically reasonable convergence of receptors onto pyramidal cells is adequate. There is no evidence for such computation although we have proposed a biologically plausible scheme.

Another biologically plausible, and not mutually exclusive, mechanism was recently proposed (Ludtke and Nelson 2006). Instead of treating the baseline P-unit spike train variability as noise, this method makes use of the statistical structure of the spike train and uses the conditional probabilities of spike discharge for very sensitive encoding of stimulus intensity. The authors suggest short-term plasticity of P-unit synapses onto pyramidal cells as a biologically plausible mechanism for estimating conditional probabilities. Again there is no evidence that such a computation is performed by the electrosensory system. More detailed physiological analyses of ELL and TS responses to prey signals will be required to test these hypotheses and potentially validate these sophisticated statistical methods as realistic approaches to weak signal detection by biological neural networks.

Third, electrocommunication signals can be high-frequency (>30 Hz) or transient signals. Although rate coding by P units might still contribute to encoding such signals (Benda et al. 2005), it is likely that temporal encoding by spike synchronization plays a far more important role in this case (Benda et al. 2006).

Fourth, *P* values have a lognormal distribution with the majority of units with probabilities between 0.16 and 0.3. The coding properties of P units vary as a function of their *P* value. Higher *P* value units have lower variance than those with low *P* values for counting windows relevant for electrolocation (<250 ms); this is especially prominent for short counting windows (<50 ms). Higher *P* values units have higher gain than those with lower *P* values (absolute spike counts only). The higher *P* value units have a stronger E1 contribution (nearly 100%) from E1 and thus code well for the time-weighted intensity; lower value P units are better at coding for rapid changes in input (E2). The higher gain and lower variability of the high *P* value units would make them very

effective in detecting weak prey signals. Target neurons in ELL might therefore improve their ability to detect prey if they could selectively sample P units with higher P values, either by selective anatomical connections or by dynamic synapses; there is no evidence that this form of optimization occurs.

P units terminate on numerous diverse pyramidal cell types in the ELL. Further, these fish are often found in foraging groups and may therefore have to simultaneously detect a wide range of environmental and communication signal frequencies. It is therefore conceivable that multiple encoding strategies are utilized by P units (e.g., both rate, ISI, and population temporal coding) and that different pyramidal cell classes differentially decode restricted codes contained within the population response: e.g., some pyramidal cells might simply integrate their P-unit input over a long time window and thus act as decoders of a rate code, whereas others might integrate over only a single EOD cycle and thus function as synchrony detectors. The electrosensory system may therefore be an ideal preparation for investigating the difficult problem of decoding population activity for a wide range of stimuli.

REFERENCES

Abbott LF, Varela JA, Sen K, Nelson SB. Synaptic depression and cortical gain control. *Science* 275: 220–224, 1997.
Adrian ED. *The Mechanism of Nervous Action.* Oxford, UK: Oxford Univ. Press, 1932.
Babineau D, Longtin A, Lewis JE. Modeling the electric field of weakly electric fish. *J Exp Biol* 209: 3636–3651, 2006.
Bastian J. Electrolocation. I. How the electroreceptors of *Apteronotus albifrons* code for moving objects and other electrical stimuli. *J Comp Physiol [A]* 144: 465–479, 1981a.
Bastian J. Electrolocation. II. The effects of moving objects and other electrical stimuli on the activities of two categories of posterior lateral line lobe cells in *Apteronotus albifrons. J Comp Physiol [A]* 144: 481–494, 1981b.
Bastian J, Chacron MJ, Maler L. Receptive field organization determines pyramidal cell stimulus-encoding capability and spatial stimulus selectivity. *J Neurosci* 22: 4577–4590, 2002.
Bastian J, Chacron MJ, Maler L. Plastic and nonplastic pyramidal cells perform unique roles in a network capable of adaptive redundancy reduction. *Neuron* 41: 767–779, 2004.
Bastian J, Courtright J. Morphological correlates of pyramidal cell adaptation rate in the electrosensory lateral line lobe of weakly electric fish. *J Comp Physiol [A]* 168: 393–407, 1991.
Bastian J, Schneiderjen S, Nguyenkim J. Arginine vasotocin modulates a sexually dimorphic communication behavior in the weakly electric fish, *Apteronotus leptorhynchus. J Exp Biol* 204: 1909–1923, 2001.
Benda J, Herz AV. A universal model for spike-frequency adaptation. *Neural Comput* 15: 2523–2564, 2003.
Benda J, Longtin A, Maler L. Spike-frequency adaptation separates transient communication signals from background oscillations. *J Neurosci* 25: 2312–2321, 2005.
Benda J, Longtin A, Maler L. A synchronization-desynchronization code for natural communication signals. *Neuron* 52: 347–358, 2006.
Bennett MVL, Sandri C, Akert K. Fine structure of the tuberous electroreceptor of the high-frequency electric fish, *Sternachus albifrons* (gymnotiformes). *J Neurocytol* 18: 265–283, 1989.

Brenner N, Bialek W, de Ruyter van Steveninck R. Adaptive rescaling maximizes information transmission. *Neuron* 26: 695–702, 2000.
Carr CE, Maler L, Sas E. Peripheral organization and central projections of the electrosensory organs in gymnotiform fish. *J Comp Neurol* 211: 139–153, 1982.
Chacron MJ. Nonlinear information processing in a model sensory system. *J Neurophysiol* 95: 2933–2946, 2006.
Chacron MJ, Longtin A, Maler L. Negative interspike interval correlations increase the neuronal capacity for encoding time-dependent stimuli. *J Neurosci* 21: 5328–5343, 2001.
Chacron MJ, Maler L, Bastian J. Electroreceptor neuron dynamics shape information transmission. *Nat Neurosci* 8: 673–678, 2005a.
Chacron MJ, Maler L, Bastian J. Feedback and feedforward control of frequency tuning to naturalistic stimuli. *J Neurosci* 25: 5521–5532, 2005b.
Chen L, House JL, Krahe R, Nelson ME. Modeling signal and background components of electrosensory scenes. *J Comp Physiol [A]* 191: 331–345, 2005.
Dayan P, Abbott L. *Theoretical Neuroscience.* Cambridge, MA: MIT Press, 2001.
de Ruyter van Steveninck RR, Bialek W. Real-time performance of a movement sensitive neuron in the blowfly visual system: coding and information transfer in short spike sequences. *Proc Roy Soc Lond B Biol Sci* 234: 379–414, 1988.
Fairhall AL, Burlingame CA, Narasimhan R, Harris RA, Puchalla JL, Berry MJ 2nd. Selectivity for multiple stimulus features in retinal ganglion cells. *J Neurophysiol* 96: 2724–2738, 2006.
Gabbiani F. Coding of time-varying signals in spike trains of linear and half-wave rectifying neurons. *Network Comput Neural Syst* 7: 61–85, 1996.
Goense JB, Ratnam R. Continuous detection of weak sensory signals in afferent spike trains: the role of anti-correlated interspike intervals in detection performance. *J Comp Physiol [A]* 189: 741–759, 2003.
Heiligenberg W, Partridge BL. How electroreceptors encode JAR eliciting stimulus regimes: reading trajectories in a phase amplitude plane. *J Comp Physiol* 142: 295–308, 1981.
Knudsen E. Behavioral thresholds to electric signals in high frequency electric fish. *J Comp Physiol* 91: 333–353, 1974.
Kreiman G, Krahe R, Metzner W, Koch C, Gabbiani F. Robustness and variability of neuronal coding by amplitude-sensitive afferents in the weakly electric fish *Eigenmannia. J Neurophysiol* 84: 189–204, 2000.
Lewis JE, Maler L. Neuronal population codes and the perception of distance in weakly electric fish. *J Neurosci* 21: 2842–2850, 2001.
Ludtke N, Nelson ME. Short-term synaptic plasticity can enhance weak signal detectability in nonrenewal spike trains. *Neural Comput* 18: 2879–2916, 2006.
MacIver MA, Sharabash NM, Nelson ME. Prey capture behavior in gymnotid electric fish: motion analysis and effects of water conductivity. *J Exp Biol* 204: 543–557, 2001.
Maler L. The posterior lateral line lobe of certain gymnotiform fish. Quantitative light microscopy. *J Comp Neurol* 183: 323–363, 1979.
Maler L, Mugnaini E. Correlating gamma-aminobutyric acidergic circuits and sensory function in the electrosensory lateral line lobe of a gymnotiform fish. *J Comp Neurol* 345: 224–252, 1994.
Maler L, Sas EK, Rogers J. The cytology of the posterior lateral line lobe of high frequency weakly electric fish (*Gymnotoidei*): dendritic differentiation and synaptic specificity in a simple cortex. *J Comp Neurol* 195: 87–139, 1981.
Metzner W, Koch C, Wessel R, Gabbiani F. Feature extraction by burst-like spike patterns in multiple sensory maps. *J Neurosci* 18: 2283–2300, 1998.
Moortgat KT, Keller CH, Bullock TH, Sejnowski TJ. Submicrosecond pacemaker precision is behaviorally modulated: the gymnotiform electromotor pathway. *Proc Natl Acad Sci USA* 95: 4684–4689, 1998.
Nelson ME. Target detection, image analysis, and modeling. In: *Electroreception*, edited by Bullock TH, Hopkins CD. New York: Springer, 2005, p. 290–317.
Nelson ME, MacIver MA. Prey capture in the weakly electric fish *Apteronotus leptorhynchus*: sensory acquisition strategies and electrosensory consequences. *J Exp Biol* 202: 1195–1203, 1999.
Nelson ME, Xu Z, Payne JR. Characterization and modeling of P-type electrosensory afferent responses to amplitude modulations in a wave-type electric fish. *J Comp Physiol [A]* 181: 532–544, 1997.
Perkel D, Bullock TH. Neural coding. In: *Neuroscience Research Program Bulletin.* Cambridge, MA: MIT Press, 1968, vol. 6, p 221–348.

Ratnam R, Nelson ME. Non-renewal statistics of electrosensory afferent spike trains: implications for the detection of weak sensory signals. *J Neurosci* 20: 6672–6683, 2000.

Saunders J, Bastian J. The physiology and morphology of two classes of electrosensory neurons in the weakly electric fish *Apteronotus Leptorhynchus*. *J Comp Physiol [A]* 154: 199–209, 1984.

Slee SJ, Higgs MH, Fairhall AL, Spain WJ. Two-dimensional time coding in the auditory brain stem. *J Neurosci* 25: 9978–9988, 2005.

Wessel R, Koch C, Gabbiani F. Coding of time-varying electric field amplitude modulations. *J Neurophysiol* 75: 2280–2293, 1996.

Xu Z, Payne JR, Nelson ME. System identification and modeling of primary electrosensory afferent response dynamics. In: *Computation in Neurons and Neural Systems*, edited by Eeckman F. New York: Kluwer Academic, 1994, p. 197–202.

Xu Z, Payne JR, Nelson ME. Logarithmic time course of sensory adaptation in electrosensory afferent nerve fibers in a weakly electric fish. *J Neurophysiol* 76: 2020–2032, 1996.

Zakon H, Oestreich J, Tallarovic S, Triefenbach F. EOD modulations of brown ghost electric fish: JARs, chirps, rises, and dips. *J Physiol* 96: 451–458, 2002.